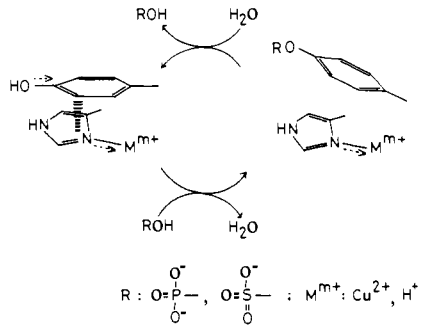

Figure 10. Proposed on–off regulation of stacking by phosphorylation or sulfation at the phenol moiety of tyr.

The importance of hydrophobic interactions in the opioid activity suggested from experiments in vitro[51] lends further support to this view.

A significant outcome of the present investigation is that the ring stacking is modulated by deprotonation of the OH group and most remarkably by its phosphorylation. The stability differences between the systems with nonphosphorylated and phosphorylated tyrosine have been determined to be 0.66–1.07 log units for various DA's, which means that phosphorylation results in nearly tenfold excess of the unstacked species over the stacked one. Because of the high pK_a value, dissociation of the tyrosine phenol OH group is difficult under physiological conditions, and accordingly the possibility of regulating the stacking in vivo by this process may be low without the aid of metal ions. Phosphorylation and sulfation by relevant kinases,[52] however, quite effectively convert the OH group to highly polar groups and may be a plausible biological choice for facile on–off switching of the stacking interaction at physiological pH (Figure 10). It is noteworthy in this context that sulfation of the tyrosyl OH group of opioid peptides greatly decreases their analgesic activity.[9] In addition to possible significance in the opioid peptide binding, stacking interactions can be an important step in enzymatic reactions such as transphosphorylation[53] and biological electron transfer.[54] Tyrosinase, a copper-containing monooxygenase that converts monophenols to diphenols,[55] has been inferred to have coordinated imidazoles at the binuclear copper site;[56] phenols as substrates may be fixed through stacking with the imidazoles as well as through the proposed direct bonding with the copper.[55b,57] Interestingly it is not benzene but phenol that is oxygenated by this enzyme.

Acknowledgment. We thank Izumi Tsuri for assistance with the experiments. This work was supported by a Grant-in-Aid for Scientific Research (No. 59470033) by the Ministry of Education, Science, and Culture, Japan, to which our thanks are due.

(51) (a) Kullmann, W. *J. Med. Chem.* **1984**, *27*, 106–115. (b) Deber, C. M.; Behnam, B. A. *Proc. Natl. Acad. Sci. U.S.A.* **1984**, *81*, 61–65. (c) Zaslavsky, B. Yu.; Mestechkina, N. M.; Miheeva, L. M.; Rogozhin, S. V.; Bakalkin, G. Ya.; Rjazhsky, G. G.; Chetverina, E. V.; Asmuko, A. A.; Bespalova, J. D. *Biochem. Pharmacol.* **1982**, *31*, 3757–3762.

(52) (a) Huttner, W. B. *Nature (London)* **1982**, *299*, 273–276. (b) Hunter, T.; Sefton, B. M. *Proc. Natl. Acad. Sci. U.S.A.* **1980**, *77*, 1311–1315.

(53) Sigel, H.; Hofstetter, F.; Martin, R. B.; Milburn, R. M.; Scheller-Krattiger, V.; Scheller, K. H. *J. Am. Chem. Soc.* **1984**, *106*, 7935–7946.

(54) (a) Guss, J. M.; Freeman, H. C. *J. Mol. Biol.* **1983**, *169*, 521–563. (b) Mauk, A. G.; Bordignon, E.; Gray, H. B. *J. Am. Chem. Soc.* **1982**, *104*, 7654–7657. (c) Quiocho, F. A.; Lipscomb, W. N. *Adv. Protein Chem.* **1971**, 1–47.

(55) (a) Lerch, K. *Met. Ions Biol. Syst.* **1981**, *13*, 143–186. (b) Solomon, E. I. "Copper Proteins"; Spiro, T. G., Ed.; Wiley-Interscience: New York, 1981; pp 41–108.

(56) Himmelwright, R. S.; Eickman, N. C.; LuBien, C. D.; Lerch, K.; Solomon, E. I. *J. Am. Chem. Soc.* **1980**, *102*, 7339–7344.

(57) Woolery, G. L.; Powers, L.; Winkler, M.; Solomon, E. I.; Lerch, K.; Spiro, T. G. *Biochim. Biophys. Acta*, **1984**, *788*, 155–161.

Polarized X-ray Absorption Edge Spectroscopy of Single-Crystal Copper(II) Complexes

Teresa A. Smith,[†] James E. Penner-Hahn,[†] Martha A. Berding,[‡] Sebastian Doniach,*[‡] and Keith O. Hodgson*[†]

Contribution from the Departments of Chemistry and Applied Physics, Stanford University, Stanford, California 94305. *Received November 14, 1984*

Abstract: Polarized X-ray absorption Cu K-edge spectra (monitored as the Cu Kα excitation fluorescence signal) have been measured on oriented single crystals of a series of square-planar Cu(II) complexes, including single-ligand species of the type CuN_4 and $CuCl_4$ and trans-mixed-ligand species of the type CuN_2Cl_2 (N = imidazole or pyridine ligands). For all complexes studied, the polarized edge spectra reveal two prominent features at ~8986 and ~8993 eV for polarizations perpendicular to the equatorial ligand plane. The positions of these sharp features change by less than 2 eV over the range of complexes studied. The spectra obtained with polarization along the in-plane Cu–ligand bonds reveal higher-energy broad or split principal maxima located between 8994 and 9001 eV. Unlike the lower-energy sharp resonance peaks, the positions of these principal maxima are strongly influenced by in-plane ligand differences and exhibit an inverse relationship to the Cu–ligand distance along the direction of polarization. Multiple-scattered-wave Xα calculations have been successful at qualitatively reproducing the prominent features of the square-planar Cu(II) polarized spectra, including the two sharp lower-energy out-of-plane-polarized features and the bond distance dependence of the in-plane polarized principal maxima. On the basis of the results of calculations and the observed orientational dependence of the edge features, the sharp resonances at 8986 and 8993 eV are assigned to a Cu 1s to $4p_z$ bound-to-bound transition and a 1s to localized continuum resonance, respectively. The higher-energy broad principal maxima observed with in-plane polarization are assigned to more delocalized continuum shape resonances.

Absorption spectra in the X-ray region are characterized by abrupt increases in the absorption coefficient, giving rise to sharp discontinuities (absorption edges). These absorption edges, resulting from the removal of a core electron, occur at characteristic threshold energies specific to a particular absorbing atom. The spectra are generally divided into two main regions: (a) the low-energy edge and near-edge region and (b) the higher-energy extended X-ray absorption fine structure (EXAFS) region, although the distinction between the regions is somewhat arbitrary.

[†] Department of Chemistry.
[‡] Department of Applied Physics.

0002-7863/85/1507-5945$01.50/0

The edge and near-edge region, typically 0–50 eV above the threshold energy, is often rich in structure resulting from transitions to unfilled valence states or continuum resonance states superimposed on the smoothly rising edge. This X-ray absorption near-edge structure (or XANES) is sensitive to the local electronic and geometric environment of the absorbing atom, and in noncubic environments, the edge features may be orientation dependent as a result of the anisotropic neighboring atom potentials.

A large number of X-ray absorption K- and L-edge spectra have been measured for transition-metal complexes. The intensity, shape, and location of observed edge features have been investigated as probes of the ligand field geometry, electronic structure, and oxidation state of the metal center.[1-11] Until recently, most X-ray absorption studies of metal complexes have been performed on polycrystalline solids or solutions. The spectra of these unoriented samples reflect a superposition of all edge transitions in both the bound-state and continuum regimes, thus making assignment of the partially resolved features quite difficult.

The high flux and plane-polarized nature of synchrotron radiation provide ideal conditions for performing polarized studies on suitable oriented single crystals. Polarized studies provide a method of resolving and orientationally selecting specific edge and near-edge features which are frequently unresolved or appear to have low intensity in the spectra of unoriented samples.[12-21] In addition, assignments of some edge features are possible based on their observed polarization properties.

In this paper we present the polarized K-edge spectra for a series of square-planar Cu(II) complexes with varying axial atom distances and in-plane ligand environments. We describe the orientation dependence of sharp edge features and the general shape and position of the edge and discuss the relationship of these features to the local geometry and electronic environment of the absorbing metal atom. The Cu(II) ion, with a d^9 electronic configuration, forms a large number of structurally characterized square-planar, square-pyramidal, and highly tetragonally elongated octahedral complexes. The square-planar geometry provides an ideal metal environment for investigating the effects of a highly anisotropic ligand field on the observed near-edge features. The isotropic K-edge spectra of many Cu(II) complexes have a shoulder or partially-resolved peak on the rising edge at ~8986 eV in addition to the 3d←1s pre-edge transition at ~8979 eV. Similar fine structure is observed in the edge spectra of other transition-metal complexes, and conflicting assignments of these features have been made.[1-9] Polarized Cu edge studies provide a basis for understanding the origins of edge features in general. They are particularly relevant to the study of Cu proteins, such as plastocyanin, for which markedly dichroic behavior has been observed recently in the sharp edge features of single crystals of this blue copper protein.[16]

Theoretical interpretation of edge features has lagged behind experimental studies, in part because the interaction of the photoelectron with the potentials of the surrounding atoms is quite complex in the low-energy near-edge region. At energies close to threshold, these interactions may be dominated by multiple scattering. Theoretical calculations in this region are, thus, much more difficult to perform than in the higher-energy EXAFS region where single scattering predominates. The first-order perturbation approximation to the potential energy resulting from single-scattering interactions described by classical EXAFS theory[22,23] is expected to break down in the threshold region. However, a recent study by Stern and Bunker[24] has found that single-scattering processes dominate even the near-edge region down to within ~13 eV of the edge. In their study, it was found that multiple scattering only became important very close to threshold or in compounds with unusually short bond distances (<1.6 Å).

Several recent theoretical studies using a multiple-scattered wave Xα formalism[25-28] have found good agreement between experimental and calculated edges for a variety of complexes and solid metals. The calculated edges include both low-energy transitions from an initial core state to a bound molecular orbital and higher-energy transitions to continuum resonance states. These resonance states reflect localized shallow potential minima which result from back-scattering of the photoelectron by the potentials of surrounding atoms. In other studies, multi-electron excitations involving shake-up and shake-down transitions[6,29,30] or plasmon excitations[31,32] have been invoked to explain fine structure in transition-metal X-ray absorption edges. Despite this progress in the interpretation of near-edge features, a more thorough knowledge of the origins of specific edge features and the relationship of these features to electronic and geometric structure is necessary before edge spectra can be used to predict metal site geometries in systems of unknown structure.

The photoabsorption cross section may be presented as

$$\sigma = |\langle\psi_f|\hat{O}|\psi_i\rangle|^2 \quad (1)$$

where $\hat{O}$ is the transition moment operator, and ψ_f and ψ_i are the final- and initial-state wave functions, respectively. In the dipolar approximation

$$\sigma = |\langle\psi_f|\vec{e}\cdot\vec{r}|\psi_i\rangle|^2 \propto \cos^2\theta|\langle\psi_f|\vec{r}|\psi_i\rangle|^2 \quad (2)$$

where $\vec{e}$ is the direction of polarization of incoming radiation, $\vec{r}$ is the molecular transition dipole operator ($\vec{x}$, $\vec{y}$, or $\vec{z}$), and θ is the angle between $\vec{e}$ and $\vec{r}$. For K edges, the initial-state wave function is the totally symmetric 1s orbital, and the integral in (2) depends only on the polarization direction and the final-state wave function. Thus, in K-edge spectra of oriented samples the angular dependence of a particular absorption feature may be used to determine the symmetry of the final-state wave function, ψ_f. In the case where ψ_f is known, the angular dependence of a feature

(1) Srivastava, U. C.; Nigam, H. L. *Coord. Chem. Rev.* **1973**, *9*, 275–310 and references therein.
(2) Agarwal, B. K.; Bhargava, C. B.; Vishnoi,A. N.; Seth, V. P. *J. Phys. Chem. Solids* **1976**, *37*, 725–728.
(3) Kostroun, V. O.; Fairchild, C. A.; Kukkonen, C. A.; Wilkins, J. W. *Phys. Rev. B* **1976**, *13*, 3268–3271.
(4) Shulman, R. G.; Yafet, Y.; Eisenberger, P.; Blumberg, W. E. *Proc. Natl. Acad. Sci. U.S.A.* **1976**, *73*, 1384–1388.
(5) Belli, M.; Scafati, A.; Bianconi, A.; Mobilio, S.; Palladina, L.; Reale, A.; Burattini, E. *Solid State Commun.* **1980**, *35*, 355–361.
(6) Bair, R. A.; Goddard, W. A. *Phys. Rev. B* **1980**, *22*, 2767–2776.
(7) Kutzler, F. W.; Hodgson, K. O.; Doniach, S. *Phys. Rev. A* **1982**, *26*, 3020–3022.
(8) Grunes, L. A. *Phys. Rev. B* **1983**, *27*, 2111.
(9) Sham, T. K. *J. Am. Chem. Soc.* **1983**, *105*, 2269–2273.
(10) Cramer, S. P.; Eccles, T. K.; Kutzler, F. W.; Hodgson, K. O. *J. Am. Chem. Soc.* **1976**, *98*, 1287–1288.
(11) Horsley, J. A. *J. Chem. Phys.* **1982**, *76*, 1451–1458.
(12) Hahn, J. E.; Hodgson, K. O. *ACS Symp. Ser.* **1983**, *211*, 431–444.
(13) Templeton, D. H.; Templeton, L. K. *Acta. Crystallogr., Sect. A*, **1980**, *36*, 237–241.
(14) Templeton, D. H.; Templeton, L. K. *Acta. Crystallogr., Sect. A* **1982**, *38*, 62–67.
(15) Heald, S. M.; Stern, E. A. *Phys. Rev. B* **1978**, *17*, 4069–4081.
(16) Scott, R. A.; Hahn, J. E.; Doniach, S.; Freeman, H. C.; Hodgson, K. O. *J. Am. Chem. Soc.* **1982**, *104*, 5364–5369.
(17) Hahn, J. E.; Scott, R. A.; Hodgson, K. O.; Doniach, S.; Desjardins, S. R.; Solomon, E. I. *Chem. Phys. Lett.* **1982**, *88*, 595–598.
(18) Stern, E. A.; Sayers, D. E.; Lytle, F. W. *Phys. Rev. Lett.* **1976**, *37*, 298–301.
(19) Stern, E. A.; Sayers, D. E.; Dash, J. G.; Shechter, H.; Bunker, B. *Phys. Rev. Lett.* **1977**, *38*, 767–770.
(20) Cox, A. D.; Beaumont, J. H. *Philos. Mag. B* **1980**, *42*, 115–126.
(21) Kutzler, F. W.; Scott, R.A.; Berg, J.M.; Hodgson, K. O.; Doniach, S.; Cramer, S. P.; Chang, C. H. *J. Am. Chem. Soc.* **1981**, *103*, 6083–6088.
(22) Lee, P. A.; Pendry, J. B. *Phys. Rev. B* **1975**, *11*, 2795.
(23) Ashley, C. A.; Doniach, S. *Phys. Rev. B* **1975**, *11*, 1279.
(24) Bunker, G.; Stern, E. A. *Phys. Rev. Lett.* **1984**, *52*, 1990–1993.
(25) Kumar, A.; Nigam, A. N.; Srivastava, B. D. *J. Phys. C: Solid State Phys.* **1980**, *13*, 3523–3527.
(26) Greaves, G. N.; Durham, P. J.; Diakun, G.; Quinn, P. *Nature (London)* **1981**, *294*, 139–142.
(27) Bianconi, A.; Dell'Ariccia, M.; Durham, P. J.; Pendry, J. B. *Phys. Rev. B* **1982**, *26*, 6502–6508.
(28) Kutzler, F. W.; Ellis, D. E.; Morrison, T. I.; Shenoy, G. K.; Viccaro, P. J.; Montano, P. A.; Appleman, E. H.; Stein, L.; Pellin, M. J.; Gruen, D. M. *Solid State Commun.* **1983**, *46*, 803–806.
(29) Stern, E. A. *Phys. Rev. Lett.* **1982**, *49*, 1353–1356.
(30) Kosugi, N.; Yokoyama, T.; Asakuna, K.; Kuroda, H. *Chem. Phys.* **1984**, *91*, 249–256.
(31) Srivastava, K. S.; Shrivastava, R. L.; Harsh, O. K.; Kumar, V. *Ind. J. Pure Appl. Phys.* **1977**, *15*, 350–354.
(32) Srivastava, K. S.; Kumar, V.; Harsh, O. K. *Ind. J. Pure Appl. Phys.* **1981**, *19*, 398–402.

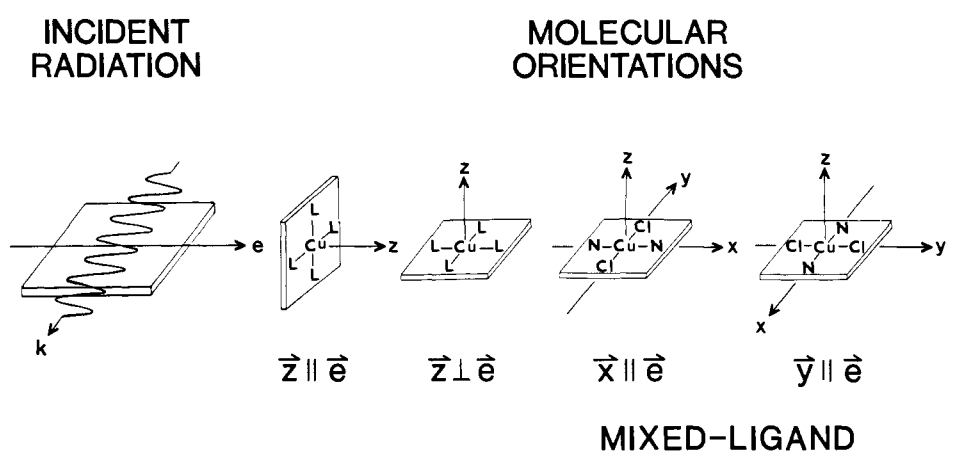

Figure 1. Summary of molecular orientations of Cu(II) square-planar complexes used to obtain *x*-, *y*-, and *z*-polarized spectra. Only the first-shell ligand environment is shown (N = imidazole or pyridine).

Table I. Structural Information on Cu Complexes

compound[a]	space group	Z	point symmetry	first-shell coordination environment	equatorial Cu–L bond length(s)[b] (Å)	closest axial atom distance (Å)	ref
$Cu(mp)_2Cl_2$	$P\bar{1}$	2	C_1	CuN_2Cl_2	Cu–N, 2.00 Cu–Cl, 2.23	Cu–Cl, 3.37	56
$CuIm_2Cl_2$	$Pbn2_1$	4	C_1	CuN_2Cl_2	Cu–N, 1.98 Cu–Cl, 2.34	Cu–Cl, 2.7	57
$(creat)_2CuCl_4$	$P2_1/c$	2	C_i	$CuCl_4$	Cu–Cl, 2.25	Cu–O, 3.64	58
$CuIm_4{\cdot}2NO_3$	$Pna2_1$	4	C_1	CuN_4	Cu–N, 2.01	Cu–O, 2.57	59
$Cu(TRI)_4{\cdot}2ClO_4$	$Pccn$	4	C_i	CuN_4	Cu–N, 2.00	Cu–O, 4.12	60

[a] Abbreviations used: mp = 2-methylpyridine; Im = imidazole; creat = creatinium; TRI = 1,4,5-trimethylimidazole. [b] Average bond lengths.

can be used to determine the nature of the transition moment operator, $\hat{O}$. This technique has been used to determine the quadrupolar nature of the 3d←1s transition in square-planar $[CuCl_4^{2-}]$.[17]

Calculations of polarized edge spectra have been performed for both the bound- and the continuum-state regions of selected Cu model complexes using a symmetry-adapted multiple-scattered-wave method and are compared to the experimental results. This type of calculation was used in a previous study of the Mo K-absorption edges of pseudotetrahedral $[MoS_2O_2^{2-}]$[21] and was found in this case to produce edge spectra in good agreement with experimental results. In the present work, we extend this calculational method to the lower-symmetry square-planar complexes.

Description of Molecular Systems

Molecular Polarizations. The complexes used in this study are square-planar Cu(II) with single-ligand coordination centers, CuN_4 and $CuCl_4$, or trans mixed-ligand centers, CuN_2Cl_2, where N refers to ligation through the N atoms of the heterocyclic planar ligands, imidazole or pyridine. The molecular axis system is defined by having the $\vec{z}$ axis perpendicular to the average CuL_4 plane (L = N, Cl). The $\vec{x}$ and $\vec{y}$ axes are defined as two orthogonal axes in this plane lying approximately along the Cu–L bonds. In the case of the mixed-ligand complexes, the $\vec{x}$ axis is defined to lie along the N–Cu–N direction and the $\vec{y}$ axis along the Cl–Cu–Cl direction. The polarized spectra presented are described by the orientation of the polarization direction ($\vec{e}$) with respect to the molecular axes, $\vec{x}$, $\vec{y}$, or $\vec{z}$. A schematic summary of the different molecular orientations is given in Figure 1.

Structural Parameters. There are several structural and electronic factors which may have an effect on the observed edge features. These include (a) the nature of the in-plane ligands, including the first ligand shell atom (N or Cl), the degree and position of substitution on the N–ligand rings, and the dihedral angles between the N–ligand planes and the CuL_4 plane; (b) the in-plane Cu–ligand bond distances; and (c) the nature and distance of the axial atoms. Systematic variations in geometry may be achieved by varying the N–ligand species (the specific ring system itself and/or the ring substitution) or the counterion used in crystallization. In this manner, a series of square-planar complexes with varying axial atom distances and in-plane ligation are obtained. In all complexes, the Cu–N bond lengths are nearly the same (2.00 ± 0.02 Å). The Cu–Cl bond lengths range from 2.23 to 2.34 Å, and the axial atom distances are between 2.57 and 4.12 Å. Table I lists the compounds studied and some of their important structural features.

The two CuN_4 imidazole complexes, $Cu(TRI)_4{\cdot}2ClO_4$ and $CuIm_4{\cdot}2NO_3$ (TRI = 1,4,5-trimethylimidazole, Im = imidazole), have significantly different axial O distances (4.12 and 2.57 Å, respectively) to the counterions. Both complexes crystallize with the imidazole ligand planes nearly perpendicular to the CuN_4 plane, with average dihedral angles of 76° and 83°, respectively. This lowers the symmetry of the Cu center from planar (D_{4h}) to inversion (C_i). The in-plane imidazole ligand environments, while very similar, differ in the number of scatterers outside the immediate CuN_4 ligand shell. The $Cu(TRI)_4$ complex has triply substituted imidazole rings with α-methyl groups ~3.4 Å from the Cu center at an angle of ~40° off the molecular z axis. The presence of these ring substituents forces the Cu–O axial interaction to be ~20° off the molecular $\vec{z}$ axis.

The $(creatinium)_2CuCl_4$ complex environment differs from the imidazole complexes in the nature and distance of the first ligand shell atoms. The nearest atom in the axial direction is a carbonyl oxygen on the creatinium cation at 3.64 Å from the Cu center.

The mixed-ligand complexes, $CuIm_2Cl_2$ and $Cu(mp)_2Cl_2$ (mp = 2-methylpyridine), while similar, exhibit some structural differences in both their in-plane ligand environments and their axial atom distance. The $CuIm_2Cl_2$ complex has unsubstituted imidazole rings which, in contrast to the CuN_4 imidazole complexes, are close to coplanar with the CuL_4 plane (tilted at ~31°). The in-plane Cu–Cl distance is rather long (2.34 Å), while the Cu–N distance (1.98 Å) is comparable to the CuN_4 case. The $Cu(mp)_2Cl_2$ complex has methyl-substituted pyridine ligands with the α-methyls located on one side of the CuL_4 plane at ~3.2 Å from the Cu center and ~37° off the molecular z axis. As in the CuN_4 imidazole complexes, the pyridine planes are close to perpendicular to the CuL_4 plane with an average dihedral angle of 78°. The in-plane Cu–L distances are closer to those observed for the single-ligand species, $CuCl_4$ and CuN_4, with a Cu–N distance of 2.00 Å and a Cu–Cl distance of 2.23 Å. In the crystal

lattice, both compounds are stacked in planes such that an equatorial Cl atom from one molecule lies in an axial position of an adjacent Cu center at 3.37 Å in $Cu(mp)_2Cl_2$ and 2.75 Å in $CuIm_2Cl_2$. In the $Cu(mp)_2Cl_2$, the sixth coordination site is blocked by the α-methyls on the opposite side of the CuL_4 plane, and in the $CuIm_2Cl_2$ complex, the closest approach of a sixth atom on the opposite side is another Cl at 4.12 Å (not indicated in Table I).

Experimental Procedure

A. Sample Preparation. All complexes except $Cu(TRI)_4 \cdot 2ClO_4$ were prepared by mixing stoichiometric amounts of Cu salts ($CuCl_2$ or $CuNO_3$) with the appropriate nitrogen ligand base and/or the counterion chloride salt in distilled water, ethanol, or methanol according to preparations described in the literature (references are listed in Table I). Single crystals of suitable size (typically 0.3–1.0 mm on a side) were obtained by slow evaporation of these solutions. Slow cooling or recrystallization was required in some cases. The $Cu(TRI)_4 \cdot 2ClO_4$ crystals were a generous gift by H. Schugar. With the exception of $Cu(mp)_2Cl_2$, crystals were mounted on glass fibers. The $Cu(mp)_2Cl_2$ crystals were mounted in a glass capillary tube together with mother liquor to inhibit previously demonstrated decomposition in the X-ray beam.

B. Crystal Alignment. All of the crystals used in this study have been structurally characterized by X-ray diffraction (see Table I for references). The published atomic coordinates were used to determine the orientation of specific molecular directions relative to the crystal axes. Integer *hkl* values corresponding to a set of lattice planes perpendicular to the chosen molecular directions were then calculated with use of the known unit cell parameters.

The general alignment procedure was to use a Syntex $P2_1$ four-circle diffractometer (Mo Kα radiation) to obtain an orientation matrix (from a rotation photograph) for each crystal. The $P2_1$ software was used to calculate the ϕ (goniometer head axis) and χ (incident beam direction) rotations required to bring the *hkl* plane of interest into a position to reflect. The $P2_1$ geometry is such that for these ϕ and χ values, the desired molecular orientation vector is perpendicular to the incoming radiation and lies in the horizontal plane. The $P2_1$ geometry was duplicated in the synchrotron experimental station. Thus, since synchrotron radiation is highly polarized in the horizontal plane, this orientation aligns the molecular vector parallel to the electric vector ($\vec{e}$) of the incoming radiation. Total uncertainties in calculated ϕ and χ positions are estimated at $\leq 2°$ as a result of rounding errors in *hkl* determinations and statistical errors in the $P2_1$ orientation matrix calculations.

The mounted crystals were supported on a Lucite two-circle goniometer which permitted rotation through $\sim 160°$ in χ and 360° in ϕ. The uncertainties in the ϕ and χ positions are approximately $\pm 2°$. Vertical and horizontal adjustment of the entire goniometer brought the crystal χ axis into alignment with the incident beam to duplicate the $P2_1$ geometry. Initial crystal positioning was accomplished optically with use of a HeNe laser beam aligned colinear with the incident X-ray beam. Crystals were then centered in the X-ray beam either by exposing a film behind the crystal and centering the crystal shadow in the beam image or by maximizing the Cu Kα fluorescence signal by small adjustments in the crystal position.

C. X-ray Absorption Measurements. X-ray absorption data were collected at Stanford Synchrotron Radiation Laboratory (SSRL) with a Si(220) double-crystal monochromator. For the majority of the complexes studied, the storage ring was operating in dedicated mode at an electron energy of 3.0 GeV with an average current of 55–70 mA. The $(creat)_2CuCl_4$ data were measured on a wiggler beam line at an electron energy of 1.8 GeV and a current of 12–15 mA. Incident and transmitted radiation was measured with N_2-filled ion chambers, and a set of Ta slits placed before the first ion chamber was used to define the beam size to 2 mm × 2 mm. A focussing mirror was used in collecting the $CuIm_2Cl_2$ and $CuIm_4 \cdot 2NO_3$ data, resulting in the lower-resolution spectra observed for these compounds.

The absorption data of single crystals were measured at room temperature as fluorescence excitation spectra, detected by an array of 4–16 NaI(Tl) scintillation detectors directed at the crystal sample. The $(creat)_2CuCl_4$ powder spectrum was measured in transmission. Data were measured from ~ 8670 to ~ 9300 eV, with a step size of approximately 0.2 eV in the edge region (8970–9050 eV). Between 2 and 5 scans were collected for each orientation.

A third ion chamber was used for internal calibration by the simultaneous measurement of the absorption of a Cu foil placed between the second and third ion chambers. The experimental spectra were energy referenced to the second maximum of the Cu foil calibrant spectrum, defined at 9004.3 eV. The position of this spectral feature is relatively unaffected by resolution differences encountered during different data runs. The reported peak locations of experimental spectra using this calibration method are accurate to approximately ±0.5 eV. Each spectrum represents the average of the individual scans, which in turn contain the weighted average of each fluorescence detector.[33] Bragg reflection peaks were observed in the scans of individual fluorescence channels for some crystal orientations. The fluorescence data for each detector were examined individually, and the Bragg peaks were removed from the spectra prior to averaging by interpolating the fluorescence scans in the energy region of the observed Bragg peaks. A smooth pre-edge background was removed from all spectra by fitting a polynomial to the pre-edge region (8670–8970 eV) and subtracting this polynomial from the entire spectrum. All edges were normalized by fitting the smooth post-edge region with a linear function and scaling the data to give a value of 1.0 for this smooth absorption extrapolated to 9000 eV.

The total X-ray exposure time was 1–6 h per crystal. X-ray diffraction peak profiles and integrated peak intensities measured before and after sample irradiation were compared to monitor any crystal degradation in the beam. Neither the diffraction peaks nor the unit cell parameters indicated significant changes in crystal integrity following synchrotron irradiation.

D. Molecular Alignment. Polarized spectra were measured at crystal orientations which maximized the projections of individual molecular vectors on the direction of polarization. The mixed-ligand complex, $Cu(mp)_2Cl_2$, belongs to the space group $P\bar{1}$. The inversion relationship between the two molecules per unit cell results in exact alignment of the two molecular $\vec{x}$, $\vec{y}$, and $\vec{z}$ axes. Alignment along these directions reflects complete $\vec{x}$, $\vec{y}$, or $\vec{z}$ polarization.

The remaining complexes crystallize in the higher symmetry space groups indicated in Table I. The directions which maximize the projection of molecular axes are the bisecting vectors of the symmetry-related molecular vectors. Table II shows the chosen alignment directions (represented by their normal [*hkl*] planes), their angular deviations from the molecular axes, and the resulting percent polarization for these orientations based on the $\cos^2 \theta$ dependency shown in eq 2. As can be seen in this table, the alignment directions for the complexes $(creat)_2CuCl_4$ and $CuIm_2Cl_2$ reflect greater than 95% polarization along the molecular axes. The $Cu(TRI)_4 \cdot 2ClO_4$ crystal orientations are less completely polarized, with $\sim 10\%$ $\vec{z}$ character in the $\vec{z} \perp \vec{e}$ orientation. The worst case for molecular misalignment is for $CuIm_4 \cdot 2NO_3$. The two oriented spectra were measured along the crystallographic *b* and *c* axes, corresponding to $\sim 64\%$ and 24% $\vec{z}$ polarization, respectively. The $\vec{z} \| \vec{e}$ and $\vec{z} \perp \vec{e}$ spectra presented for $CuIm_4 \cdot 2NO_3$ were calculated from the normalized *b* and *c* polarized spectra by taking the weighted difference of the two spectra based on the percent $\vec{z}$ character in the crystal spectra. With use of the same method, the polarized spectra for $Cu(TRI)_4 \cdot 2ClO_4$ were calculated from its *b* and *c* polarized spectra. The difference edge spectra calculated in this fashion are more sensitive to the noise level of the data, uncertainties in energy calibration, and cumulative angular errors in crystal alignment.

Table II. Molecular Axis Projections on Oriented Crystal Alignment Vectors

compound	alignment vector [*hkl*]	angular deviations of molecular axes			% polarization[a]	
		x	*y*	*z*	$\vec{z} \| \vec{e}$	$\vec{z} \perp \vec{e}$
$CuIm_4 \cdot 2NO_3$	[010]	89.4	52.4	35.9	63.8	36.2
	[001]	90.4	37.6	55.2	34.2	65.8
$Cu(TRI)_4 \cdot 2ClO_4$	[010]	67.3	29.4	71.8	9.7	90.3
	[001]	75.6	75.5	19.7	87.7	12.3
$(creat)_2CuCl_4$	[010]	8.5	82.2	84.8	0.8	99.2
	[−103]	84.8	89.9	5.1	99.2	0.8
$CuIm_2Cl_2$	[100]	3.4	87.3	86.1	0.5	99.3 *x* 0.2 *y*
	[010]	86.9	10.9	85.8	0.6	0.3 *x* 99.1 *y*
	[001]	88.6	79.4	5.7	96.6	0.1 *x* 3.3 *y*

[a] Calculated from eq 2.

Method of Calculation

Theoretical calculations were performed with a multiple-scattered-wave Xα method (MSW-Xα). This method has been described extensively elsewhere[34] and will only be briefly summarized here. The MSW-Xα method is based on a muffin-tin approximation to the molecular

(33) Cramer, S. P.; Scott, R. A. *Rev. Sci. Instrum.* **1981**, *52*, 395.
(34) Kutzler, F. W.; Natoli, C. R.; Misemer, D. K.; Doniach, S.; Hodgson, K. O. *J. Chem. Phys.* **1980**, *73*, 3274–3288.

potential in which the molecular cluster is divided into three regions. Region I consists of spheres centered about each atomic site inside which the potential is spherically averaged. Region III, the "outer sphere", is defined as the space outside of a sphere enclosing all the atomic spheres in which the potential is also spherically averaged. Region II, the "interstitial region", consists of the remaining space between the atomic and outer spheres. The potential in this region is volume averaged, giving a constant and generally negative potential, V_{II}. Due to this division of space and the averaging of the potentials, the solution to the wave equation is separable into radial and angular parts in all three regions, the angular solutions having the form of spherical harmonics. In Region II, the radial solutions can be written analytically as linear combinations of ordinary or modified spherical Neumann and Bessel functions. In Regions I and III, the radial solutions are obtained from numerical integrations on a radial mesh. The total electron energies, E, for bound states ($E < 0$) are determined from the eigenvalues of a set of homogeneous equations. Solutions exist for all energies in the continuum ($E > 0$). Both bound-state and continuum solutions are obtained by matching wave functions and first derivatives at region boundaries, utilizing reexpansion theorems of spherical harmonics and Bessel and Neumann functions. From these solutions, the basis function coefficients for all three regions are calculated.

To keep the problem to a reasonable computational size, one must usually approximate the true complex under investigation by a smaller cluster of atoms centered about the photoabsorber, Cu. In the complexes presented here, between one and three shells of Cu nearest neighbors were used (from 5 to 15 atoms). The muffin-tin radii defining region I were chosen according to the "Norman method",[35] and touching spheres were used (no overlap). The outer sphere was always chosen to be tangential to the muffin-tins of the outer most shell of atoms. If the cluster being studied was an ion, neutralizing charge was included on a "Watson sphere" such that the potential had the correct asymptotic behavior. This Watson sphere was placed at the same position as the outer sphere, and the charge was distributed uniformly on the surface. By constructing the angular basis functions from linear combinations of spherical harmonics which transform as the irreducible representations of the molecular point group, the set of equations can be block diagonalized. This reduces computation time significantly and permits the calculation of polarized spectra.

To calculate a self-consistent molecular potential, an initial approximate potential was obtained from a charge density superposition of parameterized Roothaan–Hartree–Fock atomic wave functions taken from Clementi and Roetti.[36] The Slater approximation to the exchange term was used, and Slater α values were taken from Schwartz.[37] This initial potential was used to construct a set of homogeneous equations; the energy eigenvalues were specified by the negative energies which lead to zeroes of the resulting secular determinant. An iterative procedure was used in which a new charge density and potential were generated from these eigenvalues and associated eigenvectors. This new potential was then mixed into the previous potential (from 5% to 30% of new mixed into old), and the resulting potential was then searched for eigenvalues. This procedure was continued until self-consistency was achieved according to the criteria that the eigenvalues change by less than ~0.001 Ry per successive cycle.

The solutions to the Schrödinger equation in region III for $E > 0$ were matched onto the appropriate Coulomb wave boundary conditions. The inhomogeneous set of equations in this continuum region were then solved for each outgoing wave basis function component, resulting in a set of wave function coefficients in all regions. The final state potentials used in the continuum calculations take into account the removal of the Cu 1s electron. The potentials can be either self-consistent, in which case the electron configuration of the cluster is allowed to relax to self-consistency maintaining the Cu 1s hole, or non-self-consistent, in which case Zn atomic wave functions are used to approximate this relaxation in the presence of the 1s hole.

The polarized continuum cross sections were calculated from

$$\sigma_c^{m_\gamma}(\omega) = \int_{-\infty}^{\infty} \frac{d\omega'(\Gamma/2\pi)\sigma_{m_\gamma}(\omega')}{(\omega - \omega')^2 + (\Gamma^2/4)} \quad (3)$$

$$\sigma_{m_\gamma}(\omega) = \hbar\omega \sum_{l,m} K|\langle\psi_{1,m}|rY_{1,m_\gamma}|\Psi_0\rangle|^2 \quad (4)$$

where $\Psi_{l,m}$ is the normalized final state wave function, Ψ_0 is the initial state Cu 1s wave function, $\hbar\omega$ is the energy of the incident photon, and K is a constant. These equations apply to dipole-allowed transitions from an $l = 0$ initial state, and m_γ corresponds to the polarization of the incident radiation. For comparison with experimental spectra, the calculated absorption cross sections were convolved with a Lorentzian broadening function of width Γ to account for the finite core-hole lifetime[38] and instrumental effects.

Two different methods may be used to examine the edge structure below the continuum edge ($E = 0$) position. In the first method, the final state of the Cu 1s electron is treated explicitly as a bound state ($E < 0$). Both the initial and final state wave functions are constrained to decay exponentially at infinity, and self-consistent wave functions are required. After the self-consistent ground state is found, the final state potentials for bound-to-bound cross sections are calculated by promoting the Cu 1s electron to an unfilled valence orbital of appropriate symmetry as determined by dipole selection rules. This excited-state electron configuration is then allowed to relax to self-consistency. The cross section for this bound-to-bound-type interaction can then be calculated by using an equation similar to (4) above.[39] This procedure must be repeated for each appropriate unfilled valence orbital. Since this method requires the calculation of numerous self-consistent potentials, it is necessarily time consuming and restricted to relatively small clusters.

In the second method, the final states for energies greater than V_{II} (which is negative) are treated with continuum-like boundary conditions. This "extended continuum" method involves the calculation of continuum region solutions in the absence of an outer sphere, with region II extended to infinity. The solutions in the extended region II can still be written in terms of modified spherical Bessel and Neumann functions $r(E - V_{II})^{1/2}$, which are real, and can still be matched to the correct continuum boundary conditions. This method was used not only for energies greater than zero (true continuum region) but also in the "extended continuum" energy region, where $V_{II} < E < 0$. Solutions in this region, which were treated as bound states by the first method, are now treated as continuum (unbound) solutions. Although the potentials used for the extended continuum calculations can be self-consistent, this method does not require calculation of the numerous self-consistent potentials required for true bound-to-bound calculations. Thus, it permits quick calculation of the full edge structure with use of a simply constructed approximate potential. The results presented in this paper emphasize the "extended-continuum" calculations. Self-consistent calculations were performed on some of the molecular models studied, and the results of these calculations will be elaborated in a subsequent publication.[40]

Extended and true continuum region calculations were performed on simplified molecular clusters approximating both the $CuCl_4$ and CuN_4 single-ligand complexes and the CuN_2Cl_2 mixed-ligand compounds. For all theoretical models studied, the structural parameters used in calculations were obtained from the structurally characterized experimental complexes (see Table I for structural details). In the case of the single-ligand complexes, $CuCl_4$ and CuN_4, strict D_{4h} symmetry was used, with the Cu–L bonds along the $\vec{x}$ and $\vec{y}$ axes. The $\vec{z}\|\vec{e}$ and $\vec{z}\perp\vec{e}$ polarized spectra were obtained by calculating transition cross sections to final states of a_{2u} and e_u symmetry, respectively. For the mixed-ligand model, CuN_2Cl_2, C_{2v} symmetry was used, and the $\vec{x}$, $\vec{y}$, and $\vec{z}$ polarized spectra reflect final states of b_1, b_2, and a_1 symmetry, respectively. In all calculations, the angular basis functions were truncated at $l = 5$ for all atomic centers and extended to $l = 10$ for the outer sphere. Lorentzian broadening widths, Γ (eq 3 above), were chosen for all clusters to best match the experimental spectra, and the calculated spectra presented for the mixed-ligand and single-ligand models represent Γ values of 8.0 and 2.0 eV, respectively.

In order to compare the results of true bound-state and extended continuum calculations, the amount of charge on the Watson sphere surrounding the self-consistent $CuCl_4$ cluster was varied and the energy levels were allowed to relax to self-consistency. This has the effect of shifting the eigenvalue energy levels relative to the zero of energy. When the Watson sphere charge was increased from +2 to +5, true continuum resonances were lowered in energy to the bound-state region ($E < 0$). Comparison of the spectra obtained with +2 and +5 charges indicated that the major effect of increasing the Watson sphere charge was to uniformly shift the energy positions of all edge features, leaving other qualitative and quantitative aspects of the cross section unchanged. In an analogous fashion, the Watson sphere charge was reduced from +2 to 0 in order to investigate the validity of treating the bound-state region between V_{II} and zero with continuum boundary conditions. By reducing the Watson charge to zero, all continuum-like features were raised in energy, and lower-energy resonances moved from the negative energy

(35) Norman, J. G., Jr. *J. Mol. Phys.* **1976**, *31*, 1191–1198.
(36) Clementi, E.; Roetti, C. *At. Data Nucl. Data Tables* **1974**, *14*, 177–478.
(37) Schwarz, K. *Phys. Rev. B* **1972**, *5*, 2466–2468.
(38) Kostroun, V. O.; Chen, M. H.; Crasemann, B. *Phys. Rev. A* **1971**, *3*, 533–545.
(39) Natoli, C. R.; Misemer, D. K.; Doniach, S.; Kutzler, F. W. *Phys. Rev. A* **1980**, *22*, 1104–1108.
(40) Berding, M.; Doniach, S., manuscript in progress.

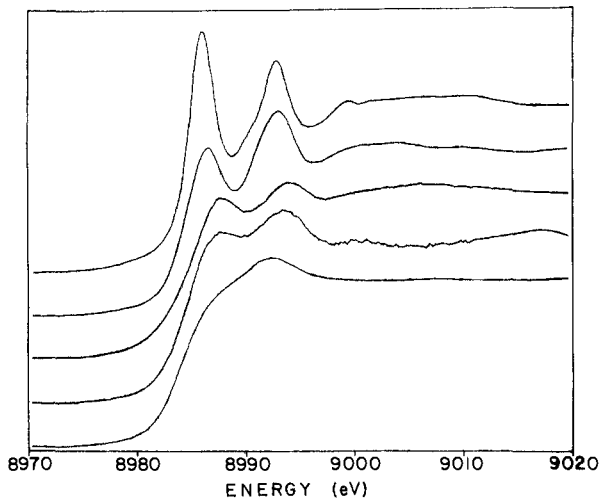

Figure 2. Comparison of highest resolution experimental $\vec{z}||\vec{e}$ spectra of all square-planar Cu(II) complexes. Top to bottom: $Cu(TRI)_4{\cdot}2ClO_4$, $(creat)_2CuCl_4$, $Cu(mp)_2Cl_2$, $CuIm_4{\cdot}2NO_3$, and $CuIm_2Cl_2$. (Full compound names are given in Table I.) The $Cu(mp)_2Cl_2$, $CuIm_4{\cdot}2NO_3$, and $CuIm_2Cl_2$ data are of comparable resolution. The higher-resolution $Cu(TRI)_4{\cdot}2ClO_4$ and $(creat)_2CuCl_4$ data may be convolved with Lorentzian broadening functions (1.2 and 0.8 eV widths, respectively) to reproduce the lower resolution of the other three compounds.

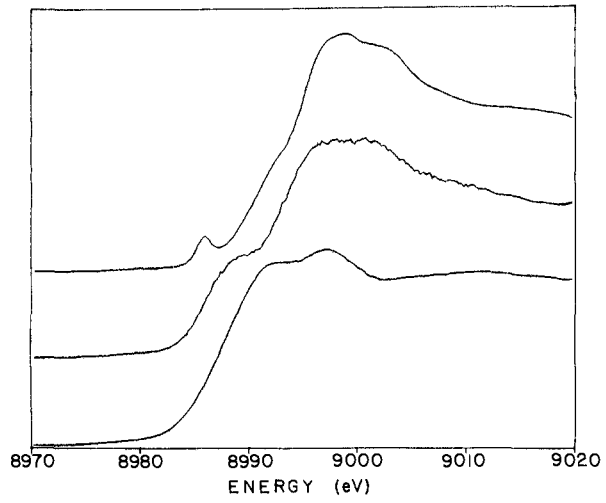

Figure 3. Comparison of the experimental $\vec{z}\perp\vec{e}$ spectra of the single-ligand complexes. Top to bottom: $Cu(TRI)_4{\cdot}2ClO_4$, $CuIm_4{\cdot}2NO_3$, and $(creat)_2CuCl_4$.

region into the true continuum region where the spherical wave boundary conditions are truly applicable. The spectra obtained with the Watson sphere charge of zero again showed only a uniform shift of all features to higher energy. The reproducibility of both the general spectral features and their relative positions in either the bound-state or continuum regimes demonstrates the utility of the extended continuum method in locating both bound-state and continuum resonances in the muffin-tin approximation.

Presentation of Results

A. Experimental Results. All of the $\vec{z}||\vec{e}$ K-edge absorption spectra have two prominent features at approximately 8986 and 8993 eV. In some complexes these features appear as sharp, intense spikes, similar in appearance to the white lines observed in $L_{2,3}$ edges. In others, they are present as partially resolved, less intense peaks. The $\vec{z}||\vec{e}$ spectra of all of the complexes are shown in Figure 2. The apparent intensity differences are due primarily to experimental resolution variation (vide infra).[41]

(41) For direct comparison with lower resolution data, 1.2 and 0.8 eV width Lorentzian broadening functions may be used to convolve the higher resolution data of $Cu(TRI)_4{\cdot}2ClO_4$ and $(creat)_2CuCl_4$, respectively. The widths of the broadening functions were determined by comparison of the internal standard Cu foil spectra.

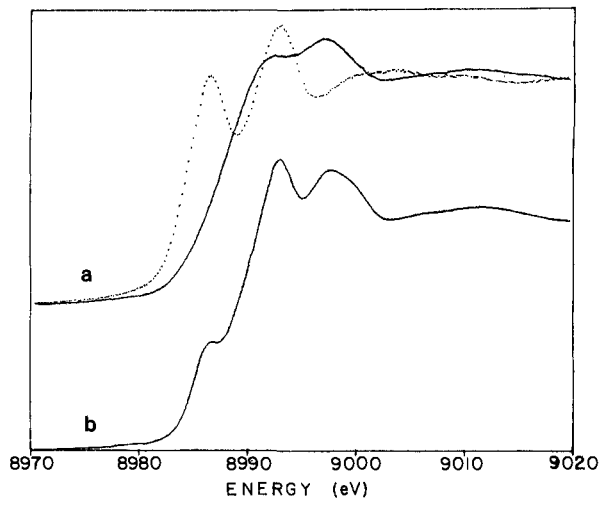

Figure 4. Comparison of polarized and unpolarized experimental spectra: (a) (···) $\vec{z}||\vec{e}$ and (—) $\vec{z}\perp\vec{e}$ polarized spectra measured on an oriented single crystal of $(creat)_2CuCl_4$; (b) powder spectrum of $(creat)_2CuCl_4$.

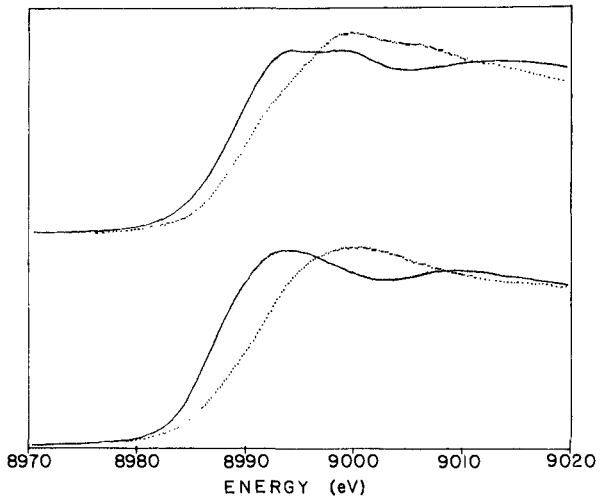

Figure 5. Cu–N$||\vec{e}$ (···) and Cu–Cl$||\vec{e}$ (—) experimental spectra of mixed-ligand complexes: upper, $Cu(mp)_2Cl_2$; lower, $CuIm_2Cl_2$.

Table III. Summary of Experimental Polarized Absorption Edge Features

compound	$\vec{z}\|\|\vec{e}$ peak energies[a] (ev)		$\vec{z}\perp\vec{e}$ peak energies[b] (eV)	
	low energy	high energy	Cu–N$\|\|\vec{e}$	Cu–Cl$\|\|\vec{e}$
$CuIm_4{\cdot}2NO_3$	8986.7	8992.9	8999[c]	
$Cu(TRI)_4{\cdot}2ClO_4$	8986.0	8992.6	9000[d]	
$(creat)_2CuCl_4$	8986.2	8992.7		8995[d]
$CuIm_2Cl_2$	8985.6	8992.5	9000[e]	8994[e]
$Cu(mp)_2Cl_2$	8987.2	8993.6	9001[c]	8997[d]

[a] Peak positons determined from the center of Lorentzian functions fit to experimental curves superimposed on a smooth arctangent background function. Accurate to within ±0.5 eV. [b] Approximate center of principal maximum determined graphically. Accurate to within ±1 eV. [c] Split nature indeterminate due to low resolution of data. [d] Detectable splitting (3.5–4.5 eV) of principal maximum at data resolution level. [e] No detectable splitting of principal maximum.

The $\vec{z}\perp\vec{e}$ spectra appear fundamentally different from the $\vec{z}||\vec{e}$ spectra, having comparatively featureless edges with broad or split principal maxima located between ~8994 and 9001 eV and lacking the sharp, lower-energy peaks observed in the $\vec{z}||\vec{e}$ spectra. Figure 3 shows $\vec{z}\perp\vec{e}$ spectra for the single-ligand Cu complexes, $Cu(TRI)_4{\cdot}2ClO_4$, $CuIm_4{\cdot}2NO_3$, and $(creat)_2CuCl_4$. Typical orientational dependence of the square-planar Cu(II) edge features can best be seen in Figure 4, which compares the $\vec{z}||\vec{c}$, $\vec{z}\perp\vec{e}$, and unpolarized edge spectra for $(creat)_2CuCl_4$. The mixed-ligand complexes, $Cu(mp)_2Cl_2$ and $CuIm_2Cl_2$, permit direct comparison

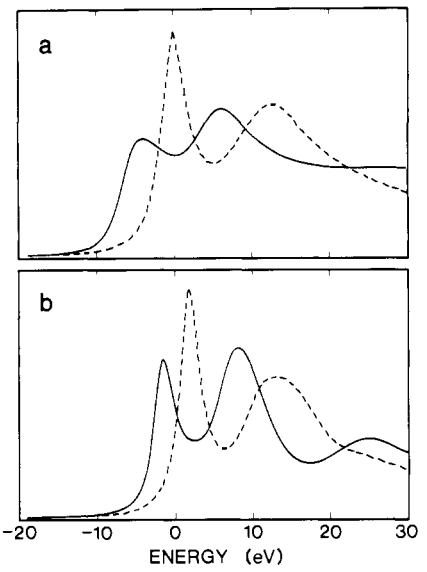

Figure 6. Calculated polarized K-edge spectra of the $CuCl_4$ models, (—) $\vec{z}||\vec{e}$ and (···) Cu–Cl$||\vec{e}$: (a) 5-atom cluster, $CuCl_4$; (b) 7-atom cluster, $CuCl_4O_2$, including axial oxygens.

of the Cu–N ($\vec{x}$) and Cu–Cl ($\vec{y}$) polarized spectra for a single molecule. These spectra are shown in Figure 5.

A summary of the prominent features in the $\vec{z}||\vec{e}$ and $\vec{z}\perp\vec{e}$ spectra of the square-planar Cu(II) complexes is given in Table III.[42]

B. Theoretical Calculations. $[CuCl_4]^{2-}$. Both self-consistent and non-self-consistent extended continuum edges were computed for the 5-atom cluster $CuCl_4$. For the self-consistent calculation, the $CuCl_4$ cluster was assigned a charge of 2– and was populated with two more electrons than required for neutrality. A neutralizing charge of 2+ was put on the Watson sphere. The self-consistent and non-self-consistent extended continuum spectra were almost identical, and only the non-self-consistent results are presented here.

To study the effects of the distant axial oxygens on the extended continuum edge features, absorption cross sections were calculated for the two non-self-consistent clusters, $CuCl_4$ and $CuCl_4O_2$, by using the Cu–Cl and Cu–O distances in the $(creat)_2CuCl_4$ compound. The resulting polarized spectra are compared in Figure 6. The observed shift of ~2 eV to higher energy for all continuum-like features upon inclusion of the axial oxygens is not significant in light of the simplified muffin-tin model which was used.

CuN_4. Three tetraimidazole models were used to study the effects of second- and third-shell scatterers on the calculated edge spectra. These models include CuN_4, $Cu(NC_2)_4$, and $Cu(NC_2)_4O_2$ clusters; in all cases, the $Cu(TRI)_4{\cdot}2ClO_4$ experimental bond distances were used. The imidazole ligands were approximated by planar NC_2 groups perpendicular to the CuN_4 plane, and the axial counter anions by oxygens in the distant axial positions. No self-consistent potentials were calculated for these clusters. The extended continuum spectra for the simplified tetraimidazole models are shown in Figure 7.

CuN_2Cl_2. Both self-consistent and non-self-consistent extended continuum calculations were done for the 5-atom cluster, $CuCl_2N_2$. As with the $CuCl_4$ cluster, the results of the two methods were similar, and only non-self-consistent results are presented. The $CuIm_2Cl_2$ bond distances were used in the calculations for CuN_2Cl_2, $Cu(NC_2)_2Cl_2$, and $Cu(NC_2)_2Cl_2(Cl_z)$ model clusters. The imidazole ligands were approximated with planar NC_2 groups

(42) The 3d ← 1s transition, which is present as a partially resolved, low intensity peak between 8978 and 8980 eV, is omitted from Table III. This feature is observed for orientations with the $\vec{e}$ and $\vec{k}$ vectors lying in the CuL_4 plane and the $\vec{e}$ vector bisecting the $\vec{x}$ and $\vec{y}$ axes. The origin of this formally dipole-forbidden transition has been discussed in a previous study,[17] and our data confirm that it is *xy* polarized and quadrupole coupled in all of the square-planar Cu(II) complexes.

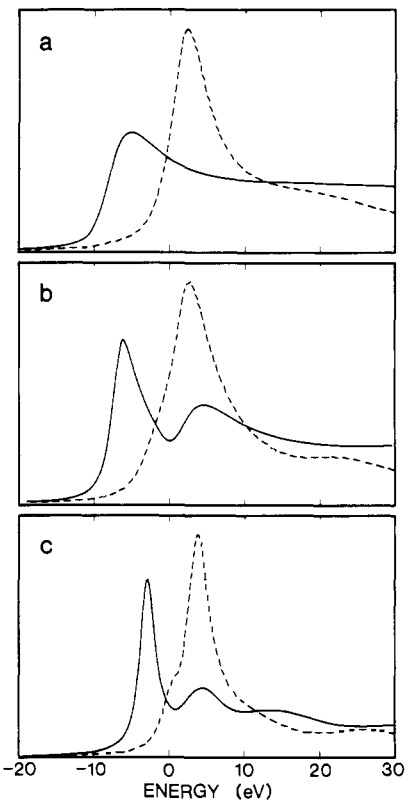

Figure 7. Calculated polarized K-edge spectra of the CuN_4 models, (—) $\vec{z}||\vec{e}$ and (···) Cu–N$||\vec{e}$: (a) 5-atom cluster, CuN_4; (b) 13-atom cluster, $Cu(NC_2)_4$, including second shell of carbons on imidazole ligands; (c) 15-atom cluster, $Cu(NC_2)_4O_2$, including second-shell carbons and axial oxygens.

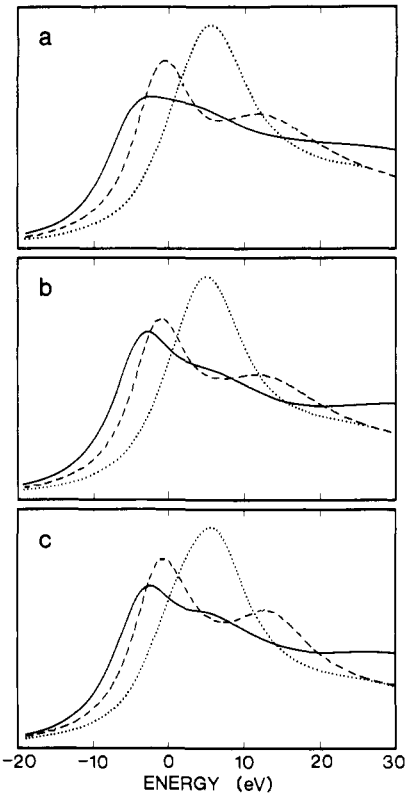

Figure 8. Calculated polarized K-edge spectra of the trans-mixed-ligand CuN_2Cl_2 models, (—) $\vec{z}||\vec{e}$, (···), Cu–N$||\vec{e}$, and (---) Cu–Cl$||\vec{e}$: (a) 5-atom cluster, CuN_2Cl_2; (b) 9-atom cluster, $Cu(NC_2)_2Cl_2$, including second shell of carbons on imidazole ligands; (c) 10-atom cluster, $Cu(NC_2)_2Cl_2Cl_z$, including second-shell carbons and one axial chlorine scatterer.

parallel to the CuL_4 plane. The resulting $\vec{x}$, $\vec{y}$, and $\vec{z}$ polarized spectra are compared in Figure 8.

Discussion

$\vec{z}||\vec{e}$ Features. The highly dichroic nature of square-planar Cu(II) complexes is clearly illustrated in the $(creat)_2CuCl_4$ spectra shown in Figure 4a. The sharp $\vec{z}$-polarized resonance features overlap with the broad main peak observed in the $\vec{z}\perp\vec{e}$ orientations, which causes the lower-energy peak (at 8986 eV) to appear as a shoulder or a weakly resolved feature in the unpolarized powder spectrum (Figure 4b). Previous studies on edges of nonoriented samples[1-3,43] have assigned this apparently low-intensity feature to a 4s←1s parity-forbidden dipole transition made allowable due to s–p mixing in the final state. This assignment was based on the assumption that the principal maximum in the K-edges of first-row transition metals corresponds to the allowed 4p←1s transition. Since the 8986-eV feature lies between the 3d←1s transition (~8980 eV) and the principal maximum, and appears to be of rather low intensity, it was assigned to a 4s←1s transition.

Parity-forbidden dipole transitions may gain intensity either through static or dynamic distortion of the inversion symmetry at the metal center, resulting in the mixing of atomic states of opposite parity, or through direct quadrupole coupling to the electromagnetic radiation.[17] In noncentrosymmetric metal complexes, enhanced intensity of the dipole-forbidden 3d←1s peak has been observed,[4] which may be explained by d–p orbital mixing in the final state of a dipole-coupled transition. However, in the centrosymmetric square-planar complexes, $(creat)_2CuCl_4$ and $Cu(TRI)_4{\cdot}2ClO_4$, and also in some octahedral complexes,[44] the 3d←1s transition has been found to be predominantly quadrupole coupled with only a small contribution from d–p vibronic coupling.

The 4s←1s transition cannot be quadrupole coupled, and in the square-planar complexes s–p mixing is forbidden by the inversion symmetry. Thus, only a vibronic coupling mechanism could be invoked to explain the presence of a 4s←1s peak. Such a transition would be expected to be very weak, with an intensity similar to the 3d←1s transitions in centrosymmetric complexes. In contrast, the 8986-eV feature is approximately 50 times more intense than the 3d←1s peak.

The intensity and $\vec{z}$-polarized nature of the 8986-eV feature are, thus, not consistent with any of the arguments proposed to explain the presence of a 4s←1s transition. The sharp features, present only in the $\vec{z}||\vec{e}$ spectra, may be assigned unambiguously to transitions involving final states of p_z character. This observation has also recently been reported by Kosugi et al. in a polarized study of $(creatinium)_2CuCl_4$.[30] In the absence of any axial ligation, the $4p_z$ orbital may be described as nonbonding in a σ-bonding sense and therefore is highly localized on the Cu center. It is thus a possible candidate for the final state in the 8986-eV transition. It is thus a possible candidate for the final state in the 8986-eV transition. Similar angularly dependent sharp edge features, polarized in the direction of least-ligand interaction, have been observed in polarized studies of some Cu(I) linear compounds[45] and the Cu–protein, plastocyanin,[16] which has a distorted trigonal pyramidal Cu center.

Our single-electron MSW-Xα calculations result in $\vec{z}||\vec{e}$ spectra which qualitatively reproduce all of the prominent experimental features. The extended continuum calculations on all model systems reveal two $\vec{z}||\vec{e}$ resonances. The first peak falls below the zero of energy, while the second feature falls above zero and, thus, in the true continuum region. True bound-state calculations on self-consistent clusters for the $CuCl_4$ and CuN_2Cl_2 models attribute the lower-energy feature to a Cu $4p_z$←1s bound-to-bound transition with some ligand orbital character in the final state.[40]

The positively charged Watson sphere technique treats both resonance features in the bound-state regime and permits a comparison of the Cu and ligand orbital character of their final states. Using this method, the first resonance is attributed to a final state composed primarily of Cu p with most of the charge density in the interstitial region. This result is consistent with the assignment of this feature as an explicit bound-to-bound transition to a Cu p_z-like final state. The second $\vec{z}||\vec{e}$ resonance region contains two states composed largely of Cl d-like character with a small admixture of Cu p and significant charge density in the outer-sphere region. This calculational result should not be viewed as an actual assignment; however, it does provide further evidence of some difference between the nature of the final states giving rise to the two $\vec{z}||\vec{e}$ features. The lower-energy feature appears as a bound-state transition using all calculational methods. The second feature appears as a continuum state resonance which, even when treated in the bound-state formalism, has a final state best described as a p_z-symmetry multiple-scattering state with some density at the Cu center.

The calculated splittings between the two $\vec{z}||\vec{e}$ resonances are between 7 and 11 eV compared to experimentally observed splittings of 6–7 eV. This discrepancy, while measurable, is not surprising in light of the muffin-tin model used. Energies of states of $\vec{z}$ symmetry are expected to be poorly modeled due to the volume-averaged potential in this region, which is comprised primarily of interstitial space.

As indicated in Figure 2 and Table III, the energies of the two sharp $\vec{z}$-polarized peaks and the splitting between them change by only a small amount as a result of either ligation changes in the CuL_4 plane or axial atom distance changes along the molecular $\vec{z}$ axis. The observed energy shifts (<2 eV) are comparable to typical shifts observed in the 3d←1s peak.[1,4] In agreement with this, the calculations (Figures 6 and 8) predict that the splitting in the two $\vec{z}||\vec{e}$ features will not change significantly as a result of axial and in-plane atom changes. The relatively fixed energies of the $\vec{z}||\vec{e}$ resonances would indicate that these features are predominantly metal centered.

An alternate theoretical interpretation of the sharp $\vec{z}||\vec{e}$ features was introduced by Bair and Goddard[6] in interpreting the unpolarized K-edge spectrum of $CuCl_2{\cdot}H_2O$, which has a planar CuO_2Cl_2 center.[46] Their theoretical method is based on a multielectron model utilizing a Hartree–Fock, configuration-interaction approach. With use of this model, the higher-energy 8993-eV feature was assigned to a pure Cu $4p_z$←1s transition and the lower-energy feature at 8986 eV to a "shake down" satellite involving a Cu $4p_z$←1s transition with simultaneous ligand-to-metal charge transfer. A similar interpretation has recently been proposed for the polarized spectra of $CuCl_2{\cdot}2H_2O$ and $(creat)_2CuCl_4$.[30,47] Our one-electron model, which allows for electron redistribution in the presence of the s core hole, effectively includes "shake down" contributions to the lowest-energy core-hole state of the molecular cluster. Such rearrangement of the valence electrons in the $4p_z$←1s final state is in fact indicated in our calculations by an increase in the percent Cu d character of calculated self-consistent core-hole states at the Fermi level.[40] Thus, if multielectron transitions are occurring which would not be accounted for by the one-electron method, they would best be described as "shake-up" transitions involving secondary electronic excitations. If such transitions were occurring, we would expect to observe experimental satellite peaks not reproduced in our theoretical spectra on the *high-energy* side of the primary $4p_z$←1s feature. As our one-electron model is able to reproduce, qualitatively, both $\vec{z}||\vec{e}$ resonances, "shake up" satellites do not seem to be important in interpreting the observed spectra with the muffin-tin model.

Satellite peaks, which are pronounced in inner-shell XPS studies of many transition-metal complexes,[48-53] are predicted to be

(43) Rao, B. J.; Chetal, A. R. *J. Phys. C: Solid State Phys.* **1982**, *15*, 6281–6284.
(44) Penner-Hahn, J. E.; Solomon, E. I.; Hodgson, K. O., manuscript in preparation.
(45) Smith, T. A.; Penner-Hahn, J. E.; Hodgson, K. O.; Berding, M. A.; Doniach, S. *Springer Proc. Phys. 2* **1984**, 58–60.
(46) Peterson, S. W.; Levy, H. A. *J. Chem. Phys.* **1957**, *26*, 220–221.
(47) Kosugi, N.; Yokoyama, T.; Asakura, K.; Kuroda, H. *Springer Proc. Phys. 2* **1984**, 55–57.
(48) Carlson, T. A.; Carver, J. C.; Saethre, L. J.; Santibanez, F. G.; Vernon, G. A. *J. Electron Spectrosc. Relat. Phenom.* **1974**, *5*, 247–258.
(49) Kono, S.; Ishii, T.; Sagawa, T.; Kobayasi, T. *Phys. Rev. Lett.* **1972**, *28*, 1385–1387.
(50) Rosencwaig, A.; Wertheim, G. K.; Guggenheim, H. J. *Phys. Rev. Lett.* **1971**, *27*, 479–481.

significantly reduced in intensity in X-ray absorption edge studies due to the shielding of the valence electrons when the photoelectron is in the low-energy threshold region.[29] A previous study using the MSW-Xα method to simulate the K-edge spectrum of $[CrO_4^{2-}]$[34] found that the one-electron model was unable to reproduce a low-intensity pre-edge feature ~7 eV above the sharp 1s to Cr (3d+4p) bound-state feature. This secondary feature may be due to a "shake up" satellite, but unlike the $\vec{z}\|\vec{e}$ resonances in the Cu(II) square-planar spectra, it has a very low intensity compared to the primary peak. Another study comparing the XPS and X-ray absorption spectra of $FeCl_2$, $MnCl_2$, and $CoCl_2$[29] found low-intensity satellites to the high-energy side of the principal absorption maxima at energies corresponding to those expected on the basis of the prominent satellite splittings found in XPS. These studies suggest that satellite structure does not easily account for the observation of two intense $\vec{z}$-polarized transitions in square-planar Cu(II). Work aimed specifically at determining the presence or absence of satellite structure in the polarized edge spectra is in progress.

Dramatic differences in the relative intensities of the 8986- and 8993-eV peaks are observed when comparing the $Cu(TRI)_4$ spectrum with those of all the other complexes studied. In the former, the 8986-eV peak is apparently more intense than the 8993-eV peak, while in all other complexes, the opposite case is observed. However, if the higher-resolution $Cu(TRI)_4$ and $(creat)_2CuCl_4$ spectra are convolved with Lorentzian broadening functions chosen to match the lower resolution of the mixed-ligand and $CuIm_4$ data,[41] the differences in relative intensities become much less pronounced. This convolution permits comparison of all of the spectra on the same resolution scale and revealed that the relative intensities of the two $\vec{z}\|\vec{e}$ features of the $Cu(TRI)_4$, $CuIm_4$, and $Cu(mp)_2Cl_2$ complexes are comparable. Although there are still observable differences in the relative intensities of the $\vec{z}\|\vec{e}$ features, the most pronounced of these (as seen in Figure 2) are due to resolution effects and not structural factors.

The structural differences between $Cu(TRI)_4$, $CuIm_4$, and $Cu(mp)_2Cl_2$ include the nature of first-shell ligands, the level of substitution on the N-ligand rings, and the axial atom distance. Unless these structural factors have counteractive effects, these structural differences do not produce significant changes in either the relative intensity or the energy of the 8986-eV feature. This observation is not easily reconciled with transitions involving ligand-to-metal charge transfer (shake down or shake up), since both intensity and energy differences would be expected for complexes with such different ligands.

The $\vec{z}\|\vec{e}$ spectrum of $CuIm_2Cl_2$, and to a lesser extent that of $CuCl_4$, shows a 8986-eV peak of somewhat lower intensity than that observed for the other complexes studied. This decrease in intensity, although difficult to quantify in low-resolution data, must be related to the in-plane ligand differences between $CuIm_2Cl_2$ and $CuCl_4$ and the other complexes studied. The $CuIm_2Cl_2$ complex is unique in its nearly coplanar arrangement of the imidazole and CuL_4 planes and its longer Cu–Cl bond distance. The orientation of the imidazole planes and their level of substitution would be expected to affect the π-bonding capabilities of the N-donor ligands. Compared to the CuN_4 complexes, a greater degree of π-overlap between the Cu $4p_z$ and ligand π orbitals is predicted with Cl ligation or with N ligation when the imidazole rings are coplanar with the CuL_4 plane. The effect of greater π overlap would be to delocalize the Cu p_z final state which gives rise to the 8986-eV peak. A reduced percent Cu $4p_z$ character in this final state would account for the decrease in the intensity of this feature.

The inclusion of second- and third-shell scatterers in the calculational models affects the calculated widths and intensities of the $\vec{z}\|\vec{e}$ features (Figures 6–8). When only nearest neighbors are included in the calculations, only the $CuCl_4$ model reveals two clearly resolved $\vec{z}\|\vec{e}$ features. In the CuN_4 and CuN_2Cl_2 models, the $\vec{z}\|\vec{e}$ spectra reveal a single broad or barely split resonance, and inclusion of the second shell of carbons on the N–ligands is required to produce the clearly split low-energy features. All of the theoretical models studied reveal that the inclusion of axial atoms in the molecular clusters results in significantly sharpened $\vec{z}\|\vec{e}$ features and the appearance of a third feature 10–16 eV above the second resonance peak. High-energy structure in the experimental $\vec{z}\|\vec{e}$ spectra is clearly evident only in the higher-resolution $Cu(TRI)_4$ data. Similar features are not observed in the spectra of the other four complexes studied. However, these data were collected with a lower monochromator resolution; hence, high-energy features may in fact be present but unresolvable.

$\vec{z}\perp\vec{e}$ Features. Examination of Figures 3 and 4 reveals that, in comparison with the $\vec{z}\|\vec{e}$ spectra, the $\vec{z}\perp\vec{e}$ spectra are characterized by relatively featureless edges displaying split or broad principal maxima located between ~8994 and 9001 eV. This principal maximum is located 4–6 eV lower in energy for orientations polarized along the Cu–Cl bond than for those polarized along the Cu–N bond. The Cu–Cl polarized spectra exhibit a second broad feature 15–20 eV above the first principal maximum. The position of the principal maximum and general edge shape in the $\vec{z}\perp\vec{e}$ spectra are affected much more strongly by the nature and distance of the in-plane ligands than are the features of the corresponding $\vec{z}\|\vec{e}$ spectra.

The $\vec{z}\perp\vec{e}$ spectra of the two CuN_4 complexes are similar in shape and edge position (see Figure 3). The $Cu(TRI)_4$ principal maximum appears noticeably split, which may be due to multiple scattering. High-energy fine structure, which appears to be absent in the $CuIm_4$ spectrum, may actually be present but unresolved due to the lower-energy resolution of these data. The shoulders or low-intensity features at ~8986 eV are attributed primarily to misalignment of the molecular vectors, incomplete polarization of the incident radiation, or artifacts in calculating the difference edges. There could be, however, some intensity to this feature in the $\vec{z}\perp\vec{e}$ orientations. The theoretical calculations do not show any low-energy fine structure in this region as a result of the idealized D_{4h} symmetry, which does not allow $p_{x,y}$ admixture into final states of p_z symmetry. In the real CuN_4 complexes, which have C_i symmetry, it is not possible, based on symmetry arguments, to rule out some $p_{x,y}$ admixture into the final state of the transition responsible for the 8986-eV peak.

The principal maximum in the $\vec{z}\perp\vec{e}$ spectrum of $CuCl_4$ is split into two partially resolved features at approximately 8992.5 and 8997.0 eV (see Figure 3). These features appear somewhat broader than the $\vec{z}\|\vec{e}$ features. The two peaks of the $CuCl_4$ spectrum are more pronounced than the split-maximum peaks in the higher-resolution spectrum of the $Cu(TRI)_4$ complex. Higher-resolution spectra for $(creat)_2CuCl_4$ crystals show these features to be fairly well-separated peaks.[30] The 8986-eV feature is completely absent in the $\vec{z}\perp\vec{e}$ spectrum, in contrast to the analogous spectra for the two imidazole complexes. Thus, it would appear that any p_x, p_y admixture into this 8986-eV final state is related to the presence of the *N*-donor ligands, which lowers the symmetry from nearly planar in the case of $CuCl_4$ to the more distorted CuN_4 centers of the imidazole complexes.

The effects of molecular misalignment and calculational errors resulting from noise and cumulative calibration errors may contribute significantly to the low-energy $\vec{z}\perp\vec{e}$ fine structure in the two CuN_4 imidazole complexes. In the case of the $Cu(mp)_2Cl_2$ complex, however, this effect should be negligible since the inversion-symmetry relationship between the two molecules per unit cell permits alignment of molecular vectors to within ~5°. In the dipole approximation, a 5° error in alignment still corresponds to greater than 99% polarization. Thus, the small amount of unresolved edge structure observed for this complex would appear to be an intrinsic effect of the complex environment or a measure of the incomplete polarization of the incedent beam.

It is interesting to note that the principal maxima in the $Cu(mp)_2Cl_2$ spectra are split for both the Cu–N and Cu–Cl polarized orientations. In contrast, the corresponding $CuIm_2Cl_2$ data, which

(51) Carlson, T. A.; Carver, J. C.; Vernon, G. A. *J. Chem. Phys.* **1975**, *62*, 932–935.
(52) Vernon, G. A.; Stucky, G.; Carlson, T. A. *Inorg. Chem.* **1976**, *15*, 278–284.
(53) Frost, D. C.; Ishitani, A.; McDowell, C. A. *Mol. Phys.* **1972**, *24*, 861–877.

are of comparable resolution, show no splitting in the principal maxima and no unresolved features on the rising portion of the edge. Thus, the $CuIm_2Cl_2$ complex is unique in its $\vec{z} \perp \vec{e}$ spectra as well as its $\vec{z} \| \vec{e}$ spectrum when compared to $Cu(mp)_2Cl_2$ and to the single-ligand complexes. It appears that the longer Cu–Cl distance, the more nearly coplanar arrangement of the imidazole ligands with respect to the CuL_4 plane, and the absence of imidazole ring substituents have a measurable effect on the overall ligand environment of the Cu center and, thus, the structure of the polarized edge spectra.

The calculated extended continuum spectra in Figures 6–8 show a dichroic behavior similar to that observed in the experimental curves. The $\vec{z} \perp \vec{e}$ cross sections are dominated by one major resonance peak in the continuum region in the Cu–N polarized spectra and two continuum region maxima separated by 11.5–13.5 eV in the Cu–Cl polarized spectra.

In both the Cu–Cl and Cu–N polarized spectra, the energy separation between the $\vec{z} \perp \vec{e}$ maximum and the bound-state $\vec{z}$-polarized feature is 4–6 eV smaller than that observed experimentally. For the Cu–Cl polarized spectra, the first maximum is located near the zero of energy (±1 eV) and ~1.5–3 eV above the first $\vec{z} \| \vec{e}$ feature. In contrast, the experimental spectra for most Cu–Cl$\| \vec{e}$ polarizations reveal a clearly split principal maximum, the lower shoulder of which overlaps the second $\vec{z} \| \vec{e}$ resonance. The calculated Cu–N polarized principal maximum is located 7–9 eV above the first $\vec{z} \| \vec{e}$ maximum, while the corresponding experimental features differ by 11–13 eV. These errors, as well as the absence of split peaks in the $\vec{z} \perp \vec{e}$ spectra, reflect the limitations of the muffin-tin model in studying square-planar complexes. The spherically-averaged atomic potentials and the volume-averaged interstitial potential are inadequate for modeling the "open space" in the axial region, the polarized electron density in the Cu–L bonds, and the π system and methyl substituent effects in the planar imidazole and pyridine ligands. The split maxima in the $\vec{z} \perp \vec{e}$ experimental spectra, which are not reproduced in the calculated spectra, may reflect multiple scattering effects due to more distant scatterers which were neglected in the simplified molecular cluster used in theoretical calculations.

In the solid state, there are additional scatterers outside the immediate molecular environment which are within 3–6 Å of the absorbing Cu center. These scatterers include more distant shells of atoms in the N-ligand rings, adjacent molecular units, and counterion atoms. Multiple scattered wave calculations on K edges of other solid systems have found that four shells of metal atoms out to 5 Å in the close-packed solid Cu metal[26] and three shells of scatterers out to 3.5 Å in the molecular solid KrF_2[28] are required to give a reasonable theoretical fit to the experimental edge structure. It is, therefore, not surprising that treating the Cu models as discrete centers having only one or two coordination shells does not result in reproduction of all of the experimentally observed edge structure. However, it is significant that the main spectral features are reproduced by using only one shell ($CuCl_4$) or two shells ($Cu(NC_2)_4$) of scatterers.

The most pronounced difference between the $CuCl_4$ and the CuN_4 spectra is the position of the principal maximum in the $\vec{z} \perp \vec{e}$ spectra. There are several structural differences between the CuN_4 and $CuCl_4$ complexes which may influence the overall electronic environment of the Cu center and, hence, shift the observed edge position. For polarization along the Cu–L bond, the most significant of these structural differences is the distance from the Cu center to the first ligand shell, which is 0.25 Å longer in the $CuCl_4$ complex. When compared to the relatively constant energies of the $\vec{z} \| \vec{e}$ features, the large shift in the $\vec{z} \perp \vec{e}$ maximum indicates that the $\vec{z} \perp \vec{e}$ edge features involve final states of a more delocalized nature, which are much more sensitive to metal–ligand distances.

A more direct comparison of the effect of metal–ligand bond distance on edge position may be made by examining the $\vec{x}$ (Cu–N) and $\vec{y}$ (Cu–Cl) polarized spectra of the mixed-ligand complexes, $CuIm_2Cl_2$ and $Cu(mp)_2Cl_2$ (Figure 5). By examining a single complex, the effects of the specific in-plane ligands may be isolated from other electronic and structural differences encountered in comparing the CuN_4 and $CuCl_4$ complexes. Polarization along the shorter Cu–N bond results in an apparent edge shift to higher energy compared to polarization along Cu–Cl. Shifts of ~5 and 7 eV are observed in response to Cu–N, Cu–Cl bond length differences of 0.23 and 0.36 Å for $Cu(mp)_2Cl_2$ and $CuIm_2Cl_2$, respectively.

The theoretical calculations of the relative positions of the $\vec{z} \perp \vec{e}$ continuum resonances (Figure 8) do a good job of reproducing this experimental edge shift in the mixed-ligand model. It has been suggested[54] that the energies of continuum resonances, reflecting quasi-bound states produced by the repulsive potential barrier of surrounding atoms, depend on $1/r^2$, where r is the absorber–scatterer distance. This general trend is observed in both the experimental and the calculated $\vec{x}$ and $\vec{y}$ polarized spectra but not in the corresponding $\vec{z}$-polarized spectra. This, again, illustrates the difference between the $\vec{z} \| \vec{e}$ and $\vec{z} \perp \vec{e}$ features. The former are best described as transitions to localized states and are fairly insensitive to constituent atom distances, while the latter are best described as delocalized continuum resonance states, strongly dependent on the Cu–ligand distance along the direction of polarization. Although both the higher-energy $\vec{z} \| \vec{e}$ resonance and the $\vec{z} \perp \vec{e}$ features are assigned to continuum resonances, the different bond-distance dependence of their energies indicates a significant difference in the nature of their final states. The fact that the energy of the principal maximum is dependent only on the first-shell ligand distance along the direction of polarization is consistent with its description as a single-scattering (EXAFS type) final state as proposed by Stern.[24] In contrast, the sharp $\vec{z} \| \vec{e}$ resonances are clearly due to multiple-scattering states.

The observation of large bond-distance-dependent shifts in the principal maximum raises the question of whether previously observed "edge shifts" of comparable magnitude, which were assigned to oxidation state differences in the threshold energy,[1] may in fact result primarily from bond-distance changes between compounds of different oxidation states. Consistent with this, $Fe^{II}(CN)_6$ and $Fe^{III}(CN)_6$ exhibit only small shifts in the positions of their edge features, in agreement with the small Fe–C and C–N bond distance changes between the two complexes.[4,27] Recent polarized studies of Cu(I) linear compounds[55] suggest that oxidation-state or other electronic effects can account for no more than a 2–3 eV shift in the apparent edge position between Cu(I) and Cu(II) complexes having similar ligands.

The energy of the first inflection point in the absorption spectrum is many times used to investigate the oxidation state of a metal. Our polarized studies show that these inflection point positions are influenced not only by metal oxidation states but even more so by the presence of unresolved low-energy transitions on the rising edge and/or metal–ligand bond distances in the first shell. Thus, oxidation-state assignments based on "edge position" alone are tenuous without some knowledge of geometry and/or bond-distance changes produced by the oxidation or reduction of the metal center.

Conclusions

A highly anisotropic square-planar ligand field with long axial distances produces characteristic X-ray edge and near-edge features which are similar for all of the complexes studied. Two intense z-polarized features are observed at ~8986 and 8993 eV, which are assigned to a 1s to Cu $4p_z$ bound-to-bound transition and to a 1s to localized continuum resonance of p_z symmetry, respectively. In contrast with previous suggestions, there is no evidence for a 4s←1s transition. Over the range of compounds studied, the nature and distance of the axial scatterer does not

(54) Natoli, C. R. *Springer Ser. Chem. Phys.* **1983**, *27*, 43–56.
(55) Smith, T. A.; Hodgson, K. O., manuscript in preparation.
(56) Duckworth, V. F.; Stephenson, N. C. *Acta Crystallogr., Sect. B* **1969**, *25*, 1795–1803.
(57) Lundberg, B. K. S. *Acta. Chem. Scand.* **1972**, *26*, 3977–3983.
(58) Udupa, M. R.; Krebs, B. *Inorg. Chim. Acta* **1979**, *33*, 241–244.
(59) McFadden, D. L.; MacPhail, A. T.; Gross, P. M.; Garner, C. D.; Mabbs, F. E. *J. Chem. Soc. Dalton Trans.* **1976**, 47–52.
(60) Bernarducci, E.; Bharadwaj, P. K.; Krogh-Jespersen, K.; Potenza, J. A.; Schugar, H. J. *J. Am. Chem. Soc.* **1983**, *105*, 3860–3866.

appear to have a measurable effect on the relative intensities or energies of the two prominent $\vec{z}$-polarized features. The relative intensity of the lower-energy feature is less pronounced in complexes which have enhanced p_z π-bonding capabilities of the in-plane ligands. Both observations are consistent with a $4p_z \leftarrow 1s$ assignment to the lower-energy feature. Enhanced intensity of this feature results from less ligand interaction and, thus, more purely atomic Cu p character in the p_z final state.

For polarization in the ligand plane, the X-ray absorption edge is characterized by broad or split continuum resonance transitions at energies higher than those observed for the $\vec{z}||\vec{e}$ features. The energies of the principal maxima are influenced largely by the Cu–ligand bond distance (r) along the direction of polarization. Consistent with theoretical predictions for true continuum shape resonances, these energies are related inversely to r, which indicate delocalized final states much more sensitive to the in-plane Cu–ligand distances than the more localized $\vec{z}||\vec{e}$ final states.

The single-electron multiple-scattered wave Xα method has proven successful in reproducing the qualitative features in the dichroic experimental edge spectra, including both the prominent $\vec{z}||\vec{e}$ features and the shifts in the $\vec{z}\perp\vec{e}$ principal maxima observed in response to Cu–ligand bond distance changes. The errors in the energies and intensities of calculated transitions reflect the limitations of the muffin-tin model in treating highly anisotropic molecular potentials. There is, however, no indication that multielectron transitions are required to interpret any of the prominent edge features. An extension of this work to take into account the full nonspherical corrections to the molecular potential and to include more distant scatterers in the unit cell is planned.

Acknowledgment. This work was supported by a grant from the National Science Foundation (PCM 82-08115). T.A.S. and J.E.P.-H. are recipients of National Science Foundation predoctoral fellowships. The work reported herein was performed at SSRL which is supported by the Department of Energy, Office of Basic Energy Sciences; the National Science Foundation, Division of Materials Research; and the National Institutes of Health, Biotechnology Resource Program, Division of Research Resources. The authors gratefully acknowledge Dr. Britt M. Hedman for useful discussions and assistance in crystallographic analyses.

Registry No. $CuIm_4 \cdot 2NO_3$, 33790-63-5; $Cu(TRI)_4 \cdot 2ClO_4$, 85337-05-9; $(creat)_2CuCl_4$, 70602-46-9; $Cu(Im)_2Cl_2$, 23570-18-5; $Cu(mp)_2Cl_2$, 13408-60-1.

η^1-Benzene Coordination: The Synthesis and X-ray Crystal Structure of a Novel Silver Salt of the Weakly Coordinating Carborane Anion $B_{11}CH_{12}^-$

Kenneth Shelly,[1] David C. Finster,[1] Young Ja Lee,[2] W. Robert Scheidt,[2] and Christopher A. Reed*[1]

Contribution from the Departments of Chemistry, University of Southern California, Los Angeles, California 90089-1062, and the University of Notre Dame, Notre Dame, Indiana 46556. *Received March 21, 1985*

Abstract: The silver salt of $B_{11}CH_{12}^-$ has been synthesized and crystallized from benzene and its X-ray crystal structure determined. Crystal data for $AgB_{11}CH_{12} \cdot 2C_6H_6$: orthorhombic, space group $Pb2_1a$, $Z = 4$, $a = 10.211$ (3) Å, $b = 20.806$ (3) Å, $c = 9.146$ (1) Å; $\rho_{calcd} = 1.392$ g/cm^3, $\rho_{obsd} = 1.39$ g/cm^3. Diffraction data were collected by the θ–2θ scan method. A total of 2010 reflections were used in the final structure determination; final discrepancy indices are $R_1 = 0.047$ and $R_2 = 0.059$. The structure reveals that two carborane anions are associated with each silver ion via terminal B–H bonds from the *closo*-carborane coordinated to the metal. Two molecules of benzene crystallize with the salt, one of which is coordinated to silver in a η^1 fashion with an Ag–C distance of 2.400 (7) Å, the shortest such contact ever observed. These modes of bonding support the idea that $B_{11}CH_{12}^-$ is a poorer σ doner than most anionic spectator ions in common use and portend its use as a novel noncoordinating anion.

Coordination chemistry has made extensive use of "noncoordinating" anions. Their large size frequently aids the stabilization of complex cations,[3] and their weak coordination allows the introduction of weak ligands[4] or the creation of vacant sites.[5] However, the usually noncoordinating anions of aqueous solution (ClO_4^-, SbF_6^-, $CF_3OSO_2^-$, etc.) frequently become coordinating in low dielectric solvents,[6,7] and the borates (BF_4^-, BPh_4^-) can be too reactive, either by coordination[7,8] or cleavage to form fluoride[9] or phenyl[6] containing products. A large, chemically inert anion which more nearly approaches the ideality of a truly noncoordinating anion could have wide utility in the preparative chemistry of cationic species.

Some 20 years ago a new class of counterions was synthesized.[10] These were the dinegatively charged polyhedral boranes $B_{10}H_{10}^{2-}$, $B_{12}H_{12}^{2-}$, and their halogenated analogues. These species exhibit remarkable chemical and thermal stability. To date, however, there has been very litle exploration of their possible roles as

(1) University of Southern California.
(2) University of Notre Dame.
(3) McDaniel, D. H. *Annu. Rep. Inorg. Gen. Synth.* **1972**, 293. Basolo, F. *Coord. Chem. Rev.* **1968**, *3*, 213.
(4) Kaesz, H., Ed. *Inorg. Synth.*, in preparation.
(5) Yared, Y. W.; Miles, S. L.; Bau, R.; Reed, C. A. *J. Am. Chem. Soc.* **1977**, *99*, 7076.
(6) Reed, C. A.; Mashiko, T.; Bentley, S. P.; Kastner, M. E.; Scheidt, W. R. *J. Am. Chem. Soc.* **1979**, *101*, 2948.
(7) Beck, W.; Schloter, K. *Z. Naturforsch B: Anorg. Chem. Org. Chem.* **1978**, *33*, 1214. Horn, E.; Snow, M. R. *Aust. J. Chem.* **1984**, *37*, 1375 and references therein.
(8) Schrock, R. R.; Osborn, J. A. *Inorg. Chem.* **1970**, *9*, 2339. Haines, R. J.; DuPreez, A. L. *J. Organomet. Chem.* **1975**, *84*, 357. Ananias de Carvalho, L. C.; Dartiguenave, M.; Dartiguenave, Y.; Beauchamp, A. L. *J. Am. Chem. Soc.* **1984**, *106*, 6848–6849.
(9) Reedijk, J. *Comments Inorg. Chem.* **1982**, *1*, 379.
(10) Muetterties, E. L.; Balthis, J. H.; Chia, Y. T.; Knoth, W. H.; Miller, H. C. *Inorg. Chem.* **1964**, *3*, 444. Knoth, W. H.; Miller, H. C.; Saver, J. C.; Bathis, J. H.; Chia, Y. T.; Muetterties, E. L. *Inorg. Chem.* **1964**, *3*, 159.

0002-7863/85/1507-5955$01.50/0